Radiological Physics and Technology (2024) 17:153–164
https://doi.org/10.1007/s12194-023-00761-y

RESEARCH ARTICLE

# Gold nanoparticles conjugated with epidermal growth factor and gadolinium for precision delivery of contrast agents in magnetic resonance imaging

**Suélio M. Queiroz[1] · Thaís S. Veriato[1] · Leandro Raniero[2] · Maiara L. Castilho[1]**

Received: 31 January 2023 / Revised: 1 November 2023 / Accepted: 2 November 2023 / Published online: 22 November 2023


**Abstract**
The utilization of contrast agents in magnetic resonance imaging (MRI) has become increasingly important in clinical diagnosis. However, the low diagnostic specificity of this technique is a limiting factor for the early detection of tumors. To develop a new contrast agent with a specific target for early stage tumors, we present the synthesis and characterization of a nanocontrast composed of gold nanoparticles (AuNPs), gadopentetic acid (Gd-DTPA), and epidermal growth factor (EGF). Carbodiimide-based chemistry was utilized to modify Gd-DTPA for functionalization with AuNPs. This resulted in the formation of the Au@Gd-EGF nanocontrast. The relaxation rate (1/T1) of the nanocontrast was analyzed using MRI, and cytotoxicity was determined based on cell viability and mitochondrial activity in a human breast adenocarcinoma cell line. Fourier-transform infrared spectroscopy analysis confirmed the effectiveness of carbodiimide in the formation of the Gd-DTPA-cysteamine complex in the presence of bands at 930, 1042, 1232, 1588, and 1716 $cm^{-1}$. The complexes exhibited good interactions with the AuNPs. However, the signal intensity of the Au@Gd-EGF nanocontrast was lower than that of the commercial contrast agent because the r1/r2 relaxivities of the Gd-DTPA-based contrast agents were lower than those of the gadoversetamide-based molecules. The Au@Gd-EGF nanocontrast agent exhibited good biocompatibility, low cytotoxicity, and high signal intensity in MRI with active targeted delivery, suggesting significant potential for future applications in the early diagnosis of tumors.

**Keywords** Gold nanoparticle · Magnetic resonance imaging · Epidermal growth factor · Gadopentetic acid

## 1 Introduction

Imaging techniques are important tools for the clinical diagnosis of diseases such as cancer. Magnetic resonance imaging (MRI) has been widely employed owing to its exceptional properties such as the absence of ionizing radiation, high spatial resolution, and high diagnostic sensitivity. However, the low diagnostic specificity of this technique requires the use of contrast agents to enhance detection, improve image quality, and differentiate normal from pathological tissues [1, 2]. In addition, the most commonly used contrast agents in MRI are gadolinium-based ($Gd^{3+}$), which have a high magnetic moment that results in a positive contrast and enhances the image signal in the T1-weighted pulse sequence (longitudinal relaxation time). The Gd3 + metal ion has seven unpaired electrons in the ground state that provide a large magnetic moment and increase the electronic relaxation time, which is potentially useful for nuclear relaxation in MRI [3, 4]. The free form of $Gd^{3+}$ is toxic to humans; therefore, the use of chelates is essential for the production of biologically stable Gd complexes [5, 6]. Moreover, these molecules have disadvantages, such as low relaxivity, unsatisfactory image enhancement, fast elimination from the circulatory system, and low specificity owing to their small molecular sizes. The use of high doses to overcome these limitations can lead to in vivo toxicity. Hence, the development of new contrast agents capable of overcoming these limitations is necessary [1].

✉ Maiara L. Castilho
mcastilho@univap.br

[1] Bionanotechnology Laboratory, Research and Development Institute, University of Vale do Paraíba, São José dos Campos, São Paulo 12244000, Brazil

[2] Nanosensors Laboratory, Research and Development Institute, University of Vale do Paraiba, Sao Jose dos Campos, Sao Paulo 12244000, Brazil

Nanotechnology combined with diagnostic medicine is a promising alternative for tumor detection. Among the nanomaterials used in the medical field, gold nanoparticles are extremely relevant because they exhibit properties such as low cytotoxicity, biocompatibility, easy structural modification, and functionalization with different biological molecules, peptides, proteins, or small-binding molecules, allowing for the development of nanomaterials that target specific molecules [7, 8]. Active targeting of peripheral ligands by gold nanoparticles (AuNPs), as in the case of biomolecules expressed on the surface of malignant cells, has become an important tool for detecting difficult-to-diagnose tumors [9, 10].

Epidermal growth factor receptor (EGFR) is a transmembrane protein that is overexpressed in several types of cancers, including breast, ovarian, prostate, bladder, colorectal, lung, and head and neck cancers [10]. This protein is expressed in over 60% of triple-negative breast tumors, which are associated with a worse prognosis, early recurrence after standard chemotherapy, a high frequency of metastasis to the lung, liver, and brain, and a low overall survival compared to other breast cancer subtypes. Furthermore, triple-negative breast tumors exhibit aggressive clinical behavior are refractory to current targeted therapies, and have a high rate of cell proliferation [11]. Considering that EGFR is activated by specific extracellular ligands such as the epidermal growth factor (EGF) protein, dimerization generates intracellular signals that are transduced through molecular processes, activating a signaling cascade and gene transcription. Activation of this pathway enhances cell function, which is associated with a high proliferative index, cell differentiation, and poor prognosis [12]. Thus, EGFR is an important marker for the molecular classification of tumors and can be used in targeted therapies.

Furthermore, to improve diagnostics using imaging techniques for early stage breast cancer, this study aimed to synthesize and characterize a novel nanocontrast agent specific to tumors overexpressing EGFR. The Au@Gd-EGF nanocontrast consisted of EGF protein and gadolinium complexes functionalized in AuNPs. Gadolinium-based contrast agents are actively targeted and transported by AuNPs through the EGF and have been used as alternative nanocontrast agents in MRI.

## 2 Material and methods

### 2.1 Formation of the complexes

Carbodiimide chemistry was used to modify the EGF (E9644, Sigma Aldrich, St. Louis, USA) and gadolinium diethylenetriaminepentaacetic acid (Gd-DTPA; 381667, Aldrich Chemistry, St. Louis, USA), in which the carboxylic group present in these molecules reacts with 1-ethyl-3-(3-dimethylaminopropyl) carbodiimide hydrochloride (EDC) to form an active intermediate, O-acylisourea, which can stabilize after reacting with primary amino groups, forming a peptide bond. The complexes formed with short-chain thiols exhibited excellent binding affinity to AuNPs through the formation of sulfur-metal bonds (Au–S). The EGF-α-lipoic acid complex was prepared according to the procedure reported by Lucas et al. [12]. In summary, EGF was bonded to α-lipoic acid (T5625, Sigma Life Science, St. Louis, USA) using EDC (03450, Fluka Analytical, St. Louis, USA) and the sodium salt of N-hydroxysulfosuccinimide (sulfo-NHS, 56485, Aldrich Chemistry, St. Louis, USA). In the carbodiimide reaction, the following molar ratios of reactants were used: 120 α-lipoic acid (7.8 mM), 3200 sulfo-NHS (187.5 mM), 1300 EDC (83.5 mM), and 1 EGF (16 µM), following the manufacturer's standard guidelines. In addition, α-lipoic acid and sulfo-NHS were mixed according to stoichiometric ratios and added to a 10 mM phosphate buffer solution containing EDC. After allowing the reaction to proceed for 30 min at room temperature, an NHS-ester intermediate was formed. The EGF protein (pH 7.4) was added to the reaction to form EGF-α-lipoic acid for 2 h. Sodium hydroxide (NaOH, S5881, Sigma Aldrich, St. Louis, USA) was added to raise the pH of the solution to a level above pH 9.0, regenerating the carboxylic acid groups in α-lipoic acid. The reaction mixture was purified using Amicon Ultra—0.5 mL Centrifugal Filters (UFC500324, Merck Millipore Ltd., Tullagreen, Carrigtowohill, Co. Corl, IRL), forming the EGF-α-lipoic acid complex (data was not available) [13].

The stability of the contrast agent is directly related to its chemical structure and ionic stability. Therefore, Gd-DTPA, a linear and ionic contrast agent, was used to form a complex with the carboxylic groups that were activated by EDC to bind to the primary amine group of cysteamine (M6500, Sigma Life Science, St. Louis, USA) (Fig. 1). The following molar ratios of the reactants were used: 1 Gd-DTPA, 25 sulfo-NHS, 10 EDC, and 3 cysteamine, following the manufacturer's standard guidelines. Thus, 19.2 µL of Gd-DTPA (14 mmol $L^{-1}$) was mixed with 66.0 µL of sulfo-NHS (187.5 mmol $L^{-1}$) and 60.0 µL of EDC (83.5 mmoL $L^{-1}$), and the solution was stirred for 30 min. Cysteamine (9 mmol $L^{-1}$) was added to the NHS-ester intermediate to form the Gd-DTPA-cysteamine complex under constant stirring and pH 7.4. After 2 h, NaOH (0.1 M) was added to raise the pH of the solution above pH 9.0, and the mixture was stirred for an additional 30 min to neutralize the byproducts such as urea. The complex was purified for 6 days by dialysis using a membrane with a porosity of 0.5 kDa (131090 T, Spectra/Por®, Spectrum Laboratories, Inc., CA, USA). Ultraviolet (UV)-visible and Fourier-transform infrared (FTIR)

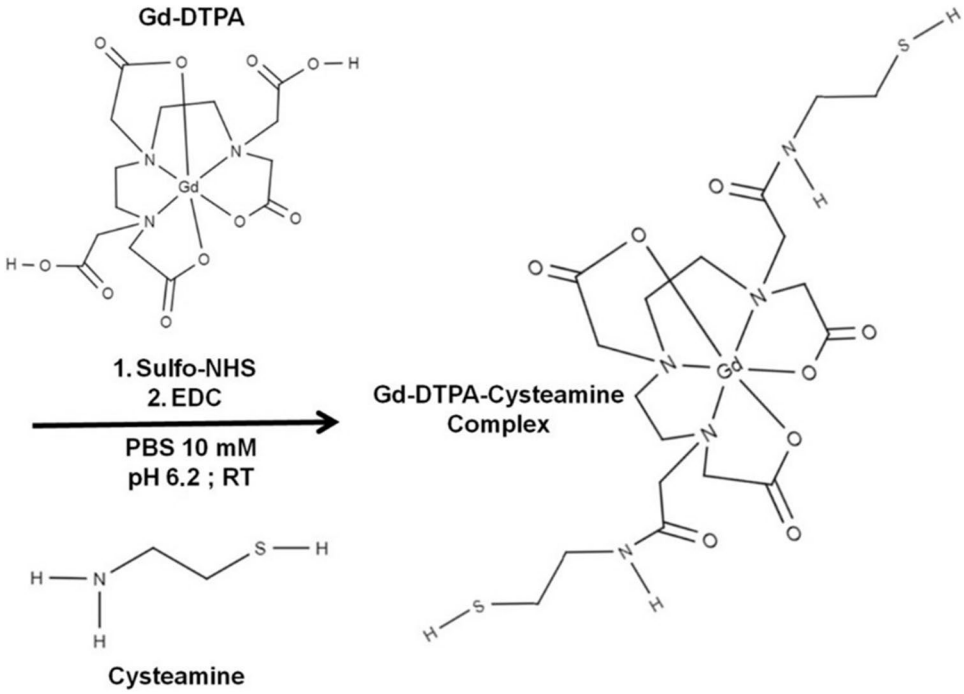


**Fig. 1** Schematic representation of the modification of Gd-DTPA via carbodiimide

spectroscopies were used to characterize the Gd-DTPA-cysteamine complex.

## 2.2 Synthesis of the Au@Gd-EGF nanocontrast

AuNPs with an average diameter of approximately 24 nm were synthesized via citrate reduction using the Lee and Meisel method [14]. Therefore, 240 mg of gold chloride trihydrate (254169, Aldrich Chemistry, St. Louis, USA) in 500 mL of ultrapure water was reduced and stabilized with 1% sodium citrate (S1804, Sigma Aldrich, St. Louis, USA) at 100 °C under constant stirring for 1 h [14, 15]. The Au@Gd-EGF nanocontrast was synthesized using the EGF-α-lipoic acid and Gd-DTPA-cysteamine complexes and functionalized on the AuNPs surface (Fig. 2). First, the EGF-α-lipoic acid complex was added to the colloidal solution and stirred for 24 h at room temperature. The Gd-DTPA-cysteamine complex was then added, and the solution was stirred constantly. After 48 h, 1 mL of the Au@Gd-EGF nanocontrast was purified by centrifugation at 6000 rpm for 6 min. The supernatant was discarded, 1 mL ultrapure water was added to the precipitate, and the nanocontrast solution was centrifuged again. The final Au@Gd-EGF pellet was diluted in ultrapure water and stored in amber bottles at 4 °C

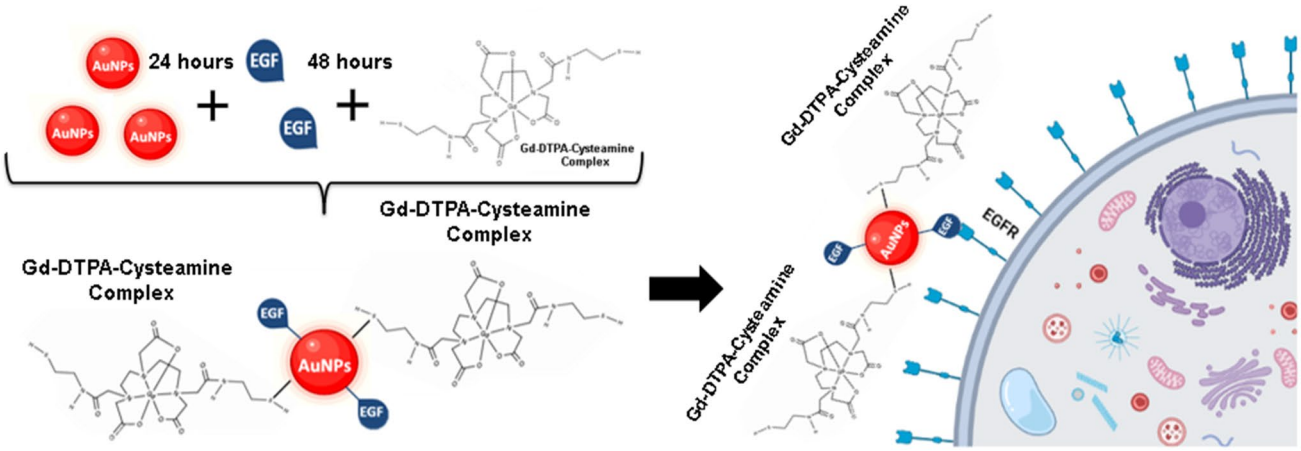


**Fig. 2** Schematic representation of gold nanoparticle functionalization with EGF and Gd-DTPA-cysteamine complex to form the Au@Gd-EGF nanocontrast

for characterization by UV–visible spectroscopy, dynamic light scattering (DLS), and FTIR spectroscopy.

### 2.3 UV–visible spectroscopy

UV–visible analyses were made on a DeNovix DS-11 spectrophotometer (DeNovix Inc., USA) at 190–840 nm with a resolution of 1 nm and 1 cm optical path length using 2 µL of each sample to characterize the AuNPs and Au@Gd-EGF nanocontrast.

### 2.4 Fourier-transform infrared spectroscopy

A 20 µL droplet of each sample was deposited on a calcium fluoride ($CaF_2$) substrate and dried in a vacuum for 30 min. FTIR spectra were obtained using a Spectrum 400 imaging system with a spotlight microscope (Perkin Elmer 400, USA) coupled to a purge system. A total of 10 spectra were collected per sample, and the acquisition parameters were 32 scans at 4 $cm^{-1}$ resolutions and a spectral range of 4000–900 $cm^{-1}$. OPUS software version 4.2 was used for statistical analysis to characterize the Gd-DTPA-cysteamine complex and Au@Gd-EGF nanocontrast.

### 2.5 Dynamic light scattering

The hydrodynamic diameters and stabilities of the AuNPs and Au@Gd-EGF nanocontrasts were measured using a Zetasizer Nano ZS90 instrument (Malvern Instruments, UK). A volume of 200 µL from each sample was added to the disposable UV microcuvette, and the parameters for size analysis were set at 21 °C, a refractive index of 1.590, and a scattering angle of 90°. The zeta potential was analyzed using 1 mL of the sample in a capillary cuvette with a DTS1070 electrode (Malvern Instruments, UK). Values were calculated as the average of three independent replicates for each set of samples.

### 2.6 MRI

The performance of the Au@Gd-EGF nanocontrast in MRI was compared with that of the benchmark formulation, OptiMARK® (Guerbet, Liebel-Flarsheim Company LLC, Raleigh, NC, USA). The samples were placed in polystyrene flasks and images were collected using a Sigma HDxt 1.5 T (GE Healthcare, USA) MRI with a skull coil and fast spin-echo T1-weighted imaging with fat saturation. The MRI parameters were as follows: axial scanning plane, inversion time (TI) = 100–400 m in increments of 20 m; repetition time (TR), 417 m; echo time (TE), 12 m; matrix size, 256 × 256; slice thickness, 3 mm; and field of view (FOV), 21 mm. The longitudinal relaxation (R1) times were obtained using Eq. (1), where signal intensity (SI) (TI) denotes the average SI as a function of TI, $SI_{inf}$ is the SI of the spin system in thermal equilibrium, and k is the cosine of the excitation angle of the inversion pulse [16]. The relaxation value of R1 was constructed as 1/longitudinal relaxation time (1/T1, $s^{-1}$) versus the Gd concentration [16].

$$SI(TI) = \left| SI_{inf}\left[1 - (1 - k) \cdot e^{-TI/T1}\right]\right| \quad (1)$$

### 2.7 Analysis of Au@Gd-EGF nanocontrast cytotoxicity

Mitochondrial activity and cell viability assays were performed to determine the cytotoxicity of the Au@Gd-EGF nanocontrast on a human breast adenocarcinoma cell line (MDA-MB-468, Rio de Janeiro Cell Bank, Brazil). In each experiment, $1 \times 10^5$ cells were seeded in 96-well plates and allowed to attach for 24 h. Different concentrations were applied at 0.1 mg $mL^{-1}$, 0.5 mg $mL^{-1}$, and 1.0 mg $mL^{-1}$, and the control cells received only culture medium. The plate was incubated for 24 h at 37 °C in a humidified atmosphere containing 95% air. The 2 mg $mL^{-1}$ tetrazolium salt [3-(4,5-dimethylthiazol-2-yl)-2,5-diphenyltetrazolium bromide] (MTT; M2128, Sigma Life Science, St. Louis, USA) solution was added to the cell plate and incubated for 4 h at 37 °C to form formazan crystals, and the absorbance was analyzed using SpectraCount™ (BS10001, Packard BioScience Company, USA). To perform the cell viability analysis, the cells were stained with 0.4% trypan blues solution (T6146, Sigma Life Science, St. Louis, USA) for 5 min and washed twice with 200 µL f saline (PBS; P3813, Sigma Aldrich, St. Louis, USA) at 0.01 M. Images were acquired using Future WinJoe version 1.0.7.9, with an inverted microscope NIB-100 (Bel Equipamentos, Piracicaba, SP, Brazil). Data were statistically analyzed using GraphPad Prism 8.0.1 software. One-way ANOVA variance was used to evaluate the effects of different variables with Tukey's multiple post hoc comparisons ($p < 0.05$).

## 3 Results

The formation of the Gd-DTPA-cysteamine and EGF-α-lipoic acid complexes through carbodiimide chemistry allowed functionalization of AuNP by the thiol radical, which led to the formation of the Au@Gd-EGF nanocontrast. FTIR spectroscopy was used to analyze changes in the molecular structure after the carbodiimide reaction. However, the byproducts of the reaction induced the agglomeration of AuNPs (Fig. 3a, blue microtube) and obscured the true absorption bands of the complex, hindering the production of the nanocontrast, thereby requiring complex purification. Dialysis was performed to purify

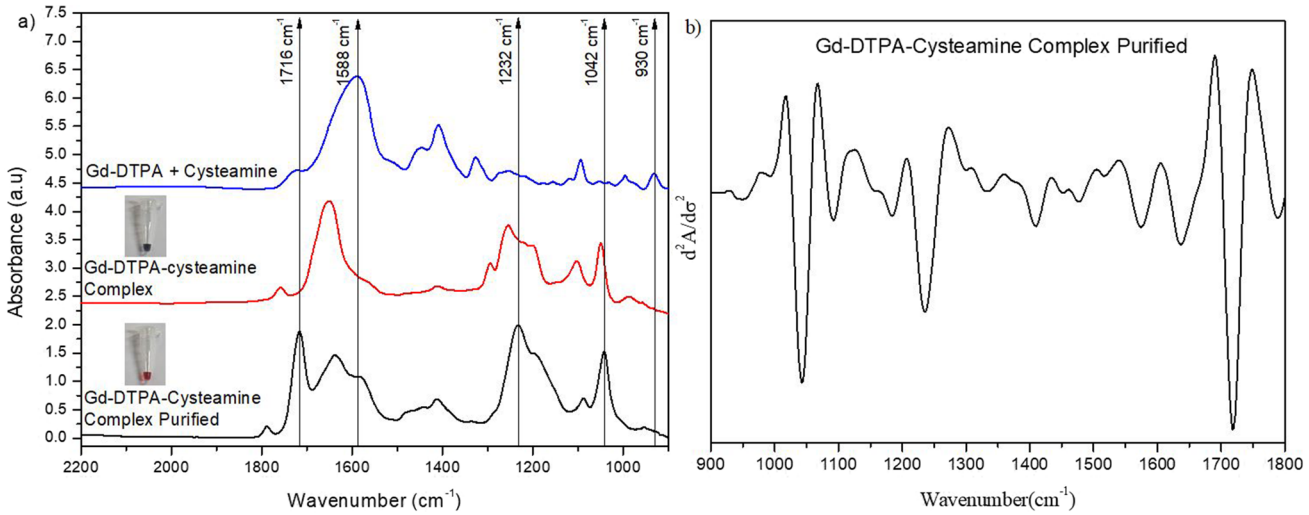


**Fig. 3** Characterizations of the Gd-DTPA-cysteamine complex; **a** FTIR ($CaF_2$) spectra of Gd-DTPA + cysteamine; Gd-DTPA-cysteamine complexes, and Gd-DTPA-cysteamine after dialysis (900–2200 $cm^{-1}$); **b** FTIR second-derivative spectra ($\frac{d^2A}{d\sigma^2}$) of purified Gd-DTPA-Cysteamine

the Gd-DTPA-cysteamine complex. The FTIR analyses showed a spectral difference between the produced complex and the purified complex (Fig. 3a), in which the byproducts of the reaction masked the real characteristic bands of the purified Gd-DTPA-cysteamine complex, corroborating the UV–visible spectroscopy analyses (Fig. S1) and revealing the presence of the reagents in the absorption region of 269 nm, which is typical of EDC, sulfo-NHS, and byproducts.

The characteristic spectrum of the purified complex consists of overlapping absorption bands of Gd-DTPA and cysteamine. Compared with the Gd-DTPA + cysteamine mixture, there were additional vibration modes in the FTIR spectrum that were indicated by the presence of bands at 930, 1042, 1232, 1588, and 1716 $cm^{-1}$. These results confirmed the chemical modification of Gd-DTPA (Fig. 3b).

The FTIR spectra presented in Fig. 4 confirmed the functionalization of the Gd-DTPA-cysteamine complex and the EGF-α-lipoic acid complex with the AuNPs to form the Au@Gd-EGF nanocontrast.

The contributions of these bands were calculated via spectral deconvolution using Gaussian curve fitting (Fig. 4a), as shown in Table 1. Data of the EGF-α-lipoic acid complex were previously recorded by Castilho et al. [10] (data not shown). The characteristic vibrational modes of the Gd-DTPA-cysteamine complex (Fig. 3b) and Au@Gd-EGF nanocontrast (Fig. 4b), as revealed by the second-derivative, were observed in the low-frequency spectra of

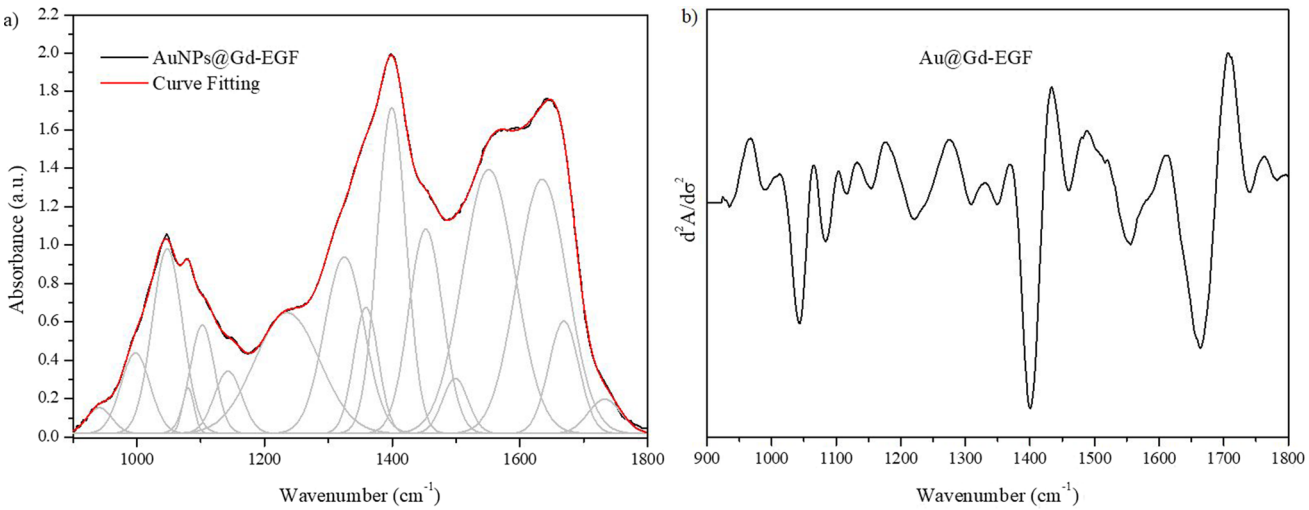


**Fig. 4** FTIR spectra of the Au@Gd-EGF nanocontrast. **a** Spectral deconvolution results of curve fitting; **b** second-derivative ($\frac{d^2A}{d\sigma^2}$)

**Table 1** Vibrational assignment by the second-derivative of the Au@Gd-EGF nanocontrast and Gd DTPA-cysteamine complex

| Wavenumber, Wn ($cm^{-1}$) | | | | | | Vibrational modes assignments |
|---|---|---|---|---|---|---|
| Au@Gd-EGF nanocontrast | | | | Gd-DTPA-cysteamine | | |
| Exp. data Wn | $\frac{d^2A}{d\sigma^2}$ | Gaussian fit | | Exp. data Wn | $\frac{d^2A}{d\sigma^2}$ | |
| | | Wn | Area | | | |
| | | | | 1788 | 1789 | $\nu$ (C=O) [17] |
| | 1742 | 1733 | 1.39 | | | $\delta$ (C=O) [18] |
| | | | | 1716 | 1718 | $\delta$ (C=O) [19] |
| | 1660 | 1669 | 4.23 | | | Amide I [20] |
| 1642 | 1637 | 1635 | 15.94 | 1637 | 1637 | $\delta$ (C=O) [19] |
| | | | | 1578 | 1574 | $\nu$ (C=O), $\nu$ (N–H) [17–20] |
| 1556 | 1554 | 1551 | 17.24 | | | Amide II [20] |
| | 1511 | 1500 | 1.76 | | 1517 | $\delta$ (N–H), $\nu$ (C–N) [21] |
| | | | | | 1478 | $\delta$ (C–H) [22] |
| | 1462 | 1453 | 8.61 | | 1451 | $\delta$ (C–H) [22] |
| 1398 | 1400 | 1400 | 11.75 | 1411 | 1409 | $\nu s$ (COO–) [23, 24] |
| | 1350 | 1359 | 3.85 | | | $\delta s$ ($CH_3$) [21] |
| | | | | | 1334 | $\delta$ (C–H) [25] |
| | 1309 | 1325 | 8.71 | | | Amide III [26] |
| | | | | | 1296 | $\nu as$ (C–O) [21] |
| 1220 | 1220 | 1236 | 9.75 | 1232 | 1236 | $\nu$ (C–N), Amide III [26] |
| | | | | 1192 | 1184 | $\nu$ (C–O) [27] |
| 1150 | 1154 | 1143 | 2.15 | | 1153 | $\nu$ (C–N) [28] |
| | 1116 | 1103 | 3.28 | | | Amide III [29] |
| 1079 | 1084 | 1080 | 0.66 | 1087 | 1092 | $\nu$ (C–N) [23] |
| 1046 | 1047 | 1047 | 6.96 | | 1042 | $\nu$ (C–N) [30] |
| | 989 | 998 | 2.94 | | 994 | $\delta$ (O–H) [21] |
| | 934 | 941 | 0.79 | 952 | 953 | $\delta$ (O–H) [21] |

$\nu$ (stretching vibration), $\delta$ (bending vibration), *s* (symmetric), *as* (asymmetric), *Wn* (wavenumber), $d^2A/d\sigma^2$ (second-derivative)

the nanocontrast from 1800 to 900 $cm^{-1}$. The nanocontrast spectrum appeared to correspond to contributions from both complexes. The Gd-DTPA-cysteamine complex dominated the spectral features of the Au@Gd-EGF according to deconvolution (Table 1).

As shown in Fig. 5, DLS measurements provide a characterization of the hydrodynamic diameter of the particles. Thus, the synthesized AuNPs presented a uniform distribution with an average diameter of 24.77 nm and a low polydispersity index (PDI) of 0.208 (Fig. 5a). The Au@Gd-EGF nanocontrast exhibited an increase in particle size of approximately 19 nm (Fig. 5b), which is consistent with the functionalization process. This increase in the hydrodynamic diameter was explained by the adsorption of the complexes onto the surface of the AuNPs, with the Gd-DTPA molecule presenting a surface area of 2.23 $nm^2$ while the EGF had an area of 9.94 $nm^2$, corroborating the data obtained in FTIR spectroscopy.

The performance of Au@Gd-EGF as a contrast agent for MRI was assessed by relaxation rate (1/T1) measurements. Thus, different concentrations of the nanocontrast and a commercial gadolinium-based contrast agent (OptiMARK®) were analyzed as presented in Fig. 6. The images showed a qualitative improvement when increasing the SI as a function of increasing concentrations of Au@Gd-EGF and OptiMARK® (Fig. 6a). Figure 6b shows the relaxation rate (1/T1) measurements according to contrast agent concentration, allowing a quantitative comparison of the R1. The R1 values of the Au@Gd-EGF nanocontrast and the commercial contrast agent were 0.77 and 3.24 $mM^{-1}$ $s^{-1}$, respectively.

The contrast agents used in MRI should exhibit low cytotoxicity. Therefore, this study evaluated the cell viability and mitochondrial activity of the nanocontrast in a human breast adenocarcinoma cell line (Fig. 7). The Au@Gd-EGF nanocontrast presented low cytotoxicity for cells exposed for 24 h of incubation at 0.1, 0.5, and 1.0 mg $mL^{-1}$, showing a survival rate higher than 75% in the MDA-MB-468 cell line, which was confirmed by the mitochondrial activity (Fig. 7a) and cell viability (Fig. 7b). Mitochondrial activity reflects the metabolic activity of cells. Although the groups

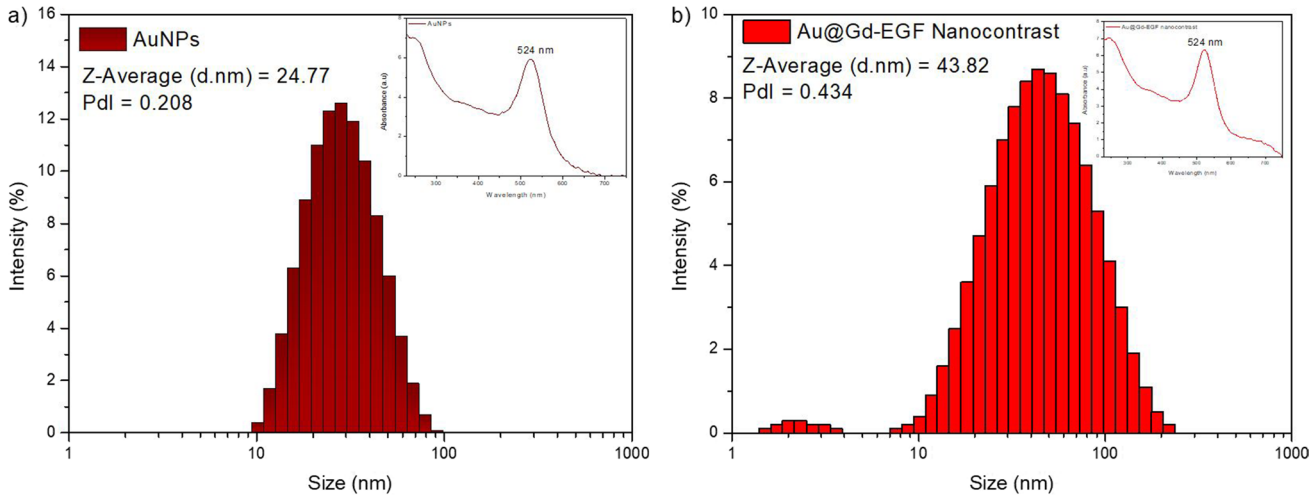


**Fig. 5** Hydrodynamic diameters and UV–visible spectra of the particles (220–750 nm); **a** AuNPs; **b** Au@Gd-EGF nanocontrast

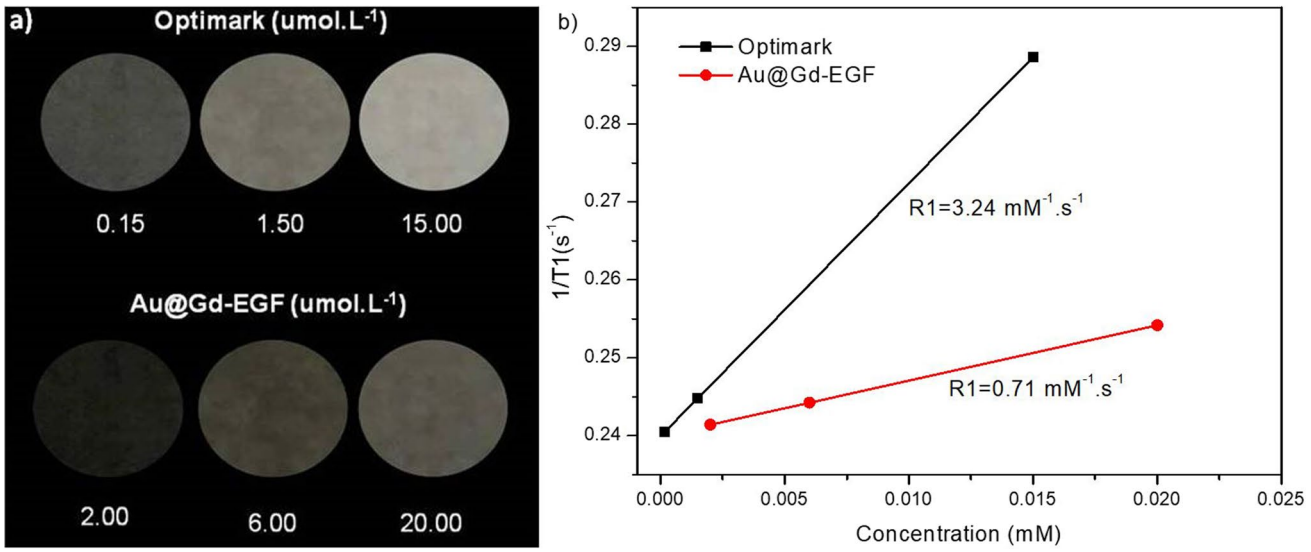


**Fig. 6** Performance of the Au@Gd-EGF nanocontrast and commercial contrast OptiMARK® in MRI. **a** T1-weighted MRI; **b** relaxation rate (1/T1)

treated with the nanocontrast showed a reduction in metabolic activity compared to the control group, the statistical analysis showed that there were no significant differences. In addition, cell viability analysis confirmed that there were no changes in cell membrane integrity, indicating low cytotoxicity.

## 4 Discussion

MRI techniques associated with the use of paramagnetic substances can be employed as alternative methods for diagnosing certain types of cancers. Although MRI has high diagnostic sensitivity, it has low diagnostic specificity, which can be overcome using nanostructured materials. Thus, this study exhibited the development of the Au@Gd-EGF nanocontrast, which presented excellent biocompatibility and low cytotoxicity and SI in MRI with active target delivery, suggesting great potential for future applications in the early diagnosis of different types of cancers that exhibit EGFR overexpression, such as breast cancer.

The vibration modes in the FTIR spectrum of the Gd-DTPA-cysteamine complex showed the formation of amide bands (1042 and 1232 $cm^{-1}$), confirming the binding between the molecules. The carboxylic acid flexion vibrations are found in regions < 1000 $cm^{-1}$. As a result, it is

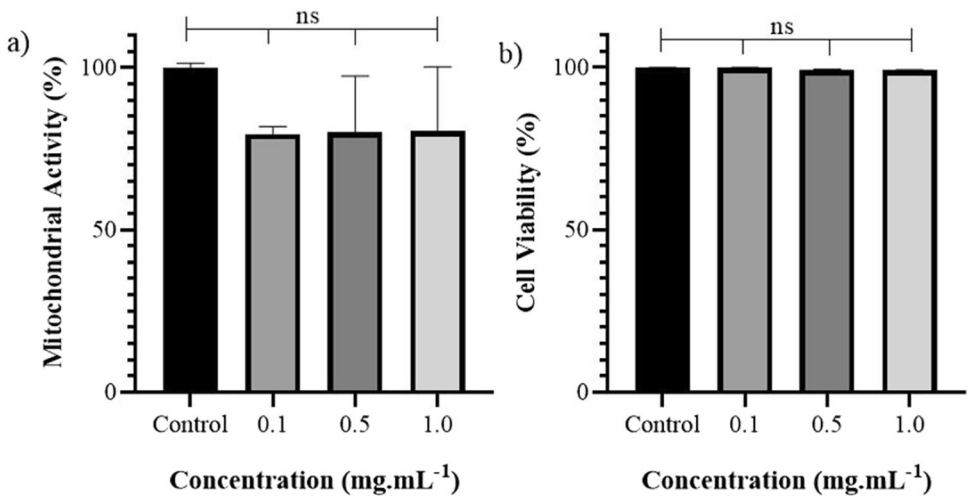


**Fig. 7** Cytotoxicity of the Au@Gd-EGF nanocontrast agent in the MDA-MB-468 cell line. **a** Mitochondrial activity; **b** cell viability. Data are expressed as the mean ± SD ($n = 3$). *ns* non-significant differences

possible to detect the presence of the functional groups of the carboxylic acids of Gd-DTPA in the spectrum of the mixture of Gd-DTPA + cysteamine at 930 $cm^{-1}$. This vibrational mode was absent after chemical modification using aqueous carbodiimide chemistry and occurred during the modification reaction of the Gd-DTPA-cysteamine complex with amide bond formation [31].

The region between 1020 and 1250 $cm^{-1}$ refers to the formation of the amide bond, corresponding to the C–N stretching vibration, where an increase in the intensity of the bands at 1042 and 1232 $cm^{-1}$ in the complex spectrum was expected since it reveals the linkage between the molecular radicals during amide formation [10, 22, 26]. The increase in the intensity of these bands indicates successful molecular modification [10]. As the Gd-DTPA + cysteamine mixture is the sum of the bands referring to the molecules, a high-intensity band is observed at 1588 $cm^{-1}$. This vibrational mode is attributed to the C–N stretch originating from Gd-DTPA [32]. In contrast, two new bands of lower intensity are formed at 1637 and 1578 $cm^{-1}$ after the formation of the amide bond between the cysteamine contrast agent, showing the presence of Gd-DTPA (C–N) and the N–H bond from the carbodiimide pathway, respectively [22, 26, 32, 33]. The carbonyl group (C=O) was modified with an amide bond formed by chemical modification of the Gd-DTPA molecule. Thus, the strong vibrational mode observed at 1716 $cm^{-1}$ in the Gd-DTPA-cysteamine complex probably refers to C=O bond weakening, resulting in a higher dipole moment [10].

Deconvolution of the Au@Gd-EGF nanocontrast FTIR spectra corresponding to the interaction of AuNPs with the complexes revealed the contributions of these bands (Table 1). The vibrational modes at 1742 and 1733 $cm^{-1}$ were assigned to the C=O stretching vibrations that may originate from esters or amides of the EGF protein [18]. The EGF-α-lipoic acid complex exhibits several amide bonds found in the backbone of EGF. The vibration of the Amide I region (1700–1600 $cm^{-1}$) results from the C=O stretching vibration related to the conformation of reverse turns, which is the inversion of the peptide chains [17–20, 22, 33]. Amide II vibrates at 1551 $cm^{-1}$ as a result of the N–H bending (60%) and C–N stretching (40%) of the proteins, and the Amide III band (1200–1350 $cm^{-1}$) is usually weak but arises predominantly from the C–N stretching vibrations coupled to N–H in-plane bending vibrations [20, 21, 25, 26]. The absorption bands at 1517, 1511, and 1500 $cm^{-1}$ are associated with amide bonds [δ (N–H) and ν(C–N)] found in the Gd-DTPA-cysteamine complex due to the modification of the molecule [20]. The Amide II mode, correlated with EGF, also exhibited absorption in this spectral region, forming overlapping bands. The spectral region from 1485 to 1445 $cm^{-1}$ of C–H bending modes refers to the molecular structure of the Gd-DTPA-cysteamine complex. The symmetric axial deformation of (COO–) at around 1400 $cm^{-1}$ corresponds to coordinated carboxyl groups [23, 24]. Bands at 1334 and 1152 $cm^{-1}$ were observed in the second-derivative spectra of the Gd-DTPA-cysteamine complex. In cysteamine, these bands are assigned as δ (C–H) and ν (C–N), respectively [25, 28, 29]. The vibration assignments of C–N are associated with Gd-DTPA at 1092, 1084, 1080, and 1079 $cm^{-1}$, evidencing the presence of this molecule in the Au@Gd-EGF nanocontrast [24, 29, 30].

DLS measurements revealed that the hydrodynamic diameters of the particles were directly related to their UV–visible spectra. The increase in nanoparticle size suggests the adsorption of EGF and Gd-DTPA molecules on their surfaces. Thus, the UV–visible spectrum of the nanocontrast presented a plasmonic resonance band centered at 524 nm, which is characteristic of AuNPs, and a small change at 250 nm, representing the Gd-DTPA region, which may be related to the functionalization of AuNPs. Li et al. [34] developed multifunctional AuNPs based on dendrimers using gadolinium as the contrast agent. The UV–visible

spectrum showed absorption at 520 nm for the AuNPs, with a small band at approximately 260 nm, corroborating the data obtained in our study [34].

Most MRI contrast agents such as Optimark produce increased signals on T1-weighted images. This is related to relaxivity, that is, the agent can increase the constant of the longitudinal (1/T1) or transverse (1/T2) relaxation rate of water normalized to the concentration of the contrast agent. However, the increased concentration of the nanocontrast agent compared to that of the commercial contrast agent leads to a decrease in SI; therefore, the optimal dose should be considered to obtain the maximum SI. In addition, for new contrast agents such as the Au@Gd-EGF nanocontrast, it is important to consider both the relaxivity of the agent and the inherent relaxation rate of the tissue, as both are involved in determining the SI [6].

The signal strength of the Au@Gd-EGF nanocontrast is lower than the commercial contrast; however, it is important to note that the relaxivities (r1/r2) of contrast media based on Gd-DTPA are lower than those of molecules based on gadoversetamide (Gd-DTPA-BMEA, OptiMARK®) [35]. The greater the ability of a gadolinium-containing molecule to induce both T1 and T2 relaxation, the greater the relaxivity of the molecule. Factors such as the concentration, molecular size, binding capacity to water molecules and human proteins, temperature, and magnetic field strength influence the relaxivity of gadolinium-containing molecules [36]. Water exchange rates play an essential role in determining the efficiency of lanthanide complexes, which consequently maximizes relaxivity to achieve high-efficiency contrast agents [37]. The low relaxivity of the nanocontrast may be related to a slow water exchange rate.

Chemical modification using carbodiimide to produce the GD-DTPA-cysteamine complex involves the binding of the functional carboxylic acid groups of GD-DTPA with the amino group present in the cysteamine molecule, forming a stable amide bond. Ferreira et al. [38] reported that amide bonds undergo slower water exchange than their parent carboxylate chelates, limiting the relaxivity that is potentially achievable by nanoparticles. Furthermore, OptiMARK® is a common contrast used in diagnostic imaging due to its low cost and high SI (T1 relaxivity @1.5T:4.4–5.0). However, they have low tumor selectivity, and non-ionic linear agents undergo 20% dissociation of $Gd^{3+}$ [39]. Heydarnezhadi et al. [40] synthesized a novel metabolic contrast agent (Gd-DTPA-DG) with a shorter T1 than that of Gd-DTPA (Magnevist) at the same concentration; however, both had little to no effect on T2. Da Silva et al. [41] analyzed gadolinium signal intensities at different concentrations and formulations. It showed an 18.52% decrease in iodinated contrasts with a pure contrast agent and a 29.26% reduction in contrast SI when diluted with xylocaine compared to gadolinium [41].

Although the modifications made to form the Gd-DTPA-cysteamine complex were different from those reported by Da Silva et al. [41], the modified Gd-DTPA signal was weaker than that of the commercial formulation, which may be a limiting factor. This corroborates the fact that the difference in the $r_1/r_2$ relaxivities between molecules, which depends on a series of combined factors, determines the efficiency of spin–lattice relaxation. In this context, the two main factors are the structure of the gadolinium chelate complex, which determines the proximity of the water molecule to the gadolinium ion, and molecular rotational dynamics [35]. Furthermore, the general rule is that a longer TR is preferred for more accurate quantification of longer T1s, whereas a shorter TR is preferable for more accurate quantification of shorter T1s. Therefore, when the T1 is much longer than the TR, the fit is unreasonable and the resulting T1 value is considered unacceptable owing to the considerable fitting error, suggesting that the T1-measurement time may have been insufficient [42].

$Gd^{3+}$ dissociation in biological systems can occur via transmetalation caused by contrast destabilization. The bond between $Gd^{3+}$ and its ligand determines the stability of the contrast agent, wherein chelation produces a molecule with a short residence time in the body. In addition to the skin, $Gd^{3+}$ is deposited in tissues, such as the brain, liver, muscle, heart, lung, pancreas, kidney, spleen, and bone. The degree of accumulation in each tissue type was unequal [39]. Epidemiological evidence suggests that the use of gadolinium-containing contrast agents may cause nephrogenic systemic fibrosis (NSF) [43]. A study conducted in patients with NSF who were administered only one type of gadolinium contrast agent throughout their lifetime revealed that a linear non-ionic agent was responsible for 438 cases of NSF after 47 million contrast administrations. Linear ionic agents caused 135 cases, with approximately twice the amount administered (95 million doses) [44]. The deposition of $Gd3^{+}$ in the brain tissue has attracted much attention from researchers. Studies have shown that detectable gadolinium deposition from macrocyclic gadolinium-based contrast agents occurs at a much higher cumulative dose than from most linear agents [39]. Moreover, the biodistribution of commercial contrast agents was homogeneous. To minimize the impact of $Gd3^{+}$ dissociation, the produced nanocontrast uses a linear gadolinium-based contrast agent functionalized to a nanoparticle with a targeting molecule to guide delivery to the region of interest. This allows for greater sensitivity and specificity of the MRI technique for the early diagnosis of breast tumors.

The specificity of nanoparticle delivery with active targeting has become an essential concept in therapeutic and diagnostic research. The active targeting of nanoparticles to particular sites in the body can be achieved using peripheral ligands that specifically bind to exposed cellular

biomolecules expressed on the surface of malignant cells with some degree of uniqueness [9, 10]. EGFR is a member of the ErbB family and comprises receptor tyrosine kinases that are internalized after ligand binding. EGFR is expressed in 14–91% of patients with breast cancer, and in several studies, it has also been associated with poor prognosis [45]. The cellular uptake and internalization of nanostructures using specific EGFR antibodies have been reported in the literature. Lucas et al. [12] assessed the binding affinity of EGFR to EGF-, EGF-linker-, and EGF-linker-coated nanoparticles, in which the nanoparticle samples showed similar responses to EGF and EGF-linker, ensuring the effectiveness of receptor-ligand binding. Creixell el al. [46] demonstrated that internalized EGF-conjugated magnetic nanoparticles targeted EGFR and significantly reduced cell viability (up to 99.9%). This may be related to the internalization of EGF-conjugated magnetic nanoparticles into MDA-MB-468 cells, which increased over time. A standard MTT assay was performed on MDA-MB-468 cells to evaluate the cytotoxicity of the Au@Gd-EGF nanocontrast. As shown in Fig. 7, no significant cytotoxicity was observed with any concentration of the nanocontrasts tested. Zhou et al. [32] evaluated the cytotoxicity of Gd-DTPAb@ZIF-8 nanoparticles in 4T1 cell lines and human umbilical vein endothelial cells where the survival rate for both cell types was over 75% after 24 h of incubation with the contrast agent at concentrations higher than 12.5 μg $mL^{-1}$ [32]. This result demonstrates the excellent biocompatibility of the Au@Gd-EGF nanocontrast agent, suggesting its applicability as a MRI contrast agent in the early diagnosis of cancer.

## 5 Conclusion

FTIR spectroscopy confirmed that the carboxylic acid groups (COOH) of gadolinium-DTPA formed an amide bond (C–N) with the primary amines ($NH_2$) present in cysteamine via a carbodiimide reaction. The significant vibrational modes at 930, 1042, 1232, 1588, and 1716 $cm^{-1}$ effectively confirmed the chemical modification of Gd-DTPA, forming a nanocontrast agent. UV–visible spectroscopy and DLS demonstrated that the complexes bind to AuNPs with high affinity, and spectral deconvolution using Gaussian curve fitting revealed bands of the complexes on the surface of the nanoparticles. Au@Gd-EGF showed sufficient relative MRI SI for diagnostic applications owing to active targeting, which allowed greater specificity and sensitivity of the technique with high efficiency. The Au@Gd-EGF nanocontrast agent exhibited good biocompatibility and low cytotoxicity and SI in MRI with active targeted delivery, suggesting a significant potential for future applications in the early diagnosis of cancer.

**Supplementary Information** The online version contains supplementary material available at https://doi.org/10.1007/s12194-023-00761-y.

**Acknowledgements** The authors would like to thank Tomovale Centro de Diagnóstico por Imagem LDTA for the MRI analyses.

**Funding** This work was supported by the grant of the FAPESP (Project 2018/23898-6), CNPq (Project 427602/2018-1 and 302994/2018-4).

## Declarations

**Conflict of interest** The authors declare that they have no known competing financial interests or personal relationships that could have appeared to influence the work reported in this paper.

## References

1. Guo C, Hu J, Bains A, Pan D, Luo K, Li N, et al. The potential of peptide dendron functionalized and gadolinium loaded mesoporous silica nanoparticles as magnetic resonance imaging contrast agents. J Mater Chem B [Internet]. 2016;4:2322–31. Available from: http://xlink.rsc.org/?DOI=C5TB02709H.
2. Clough TJ, Jiang L, Wong K-L, Long NJ. Ligand design strategies to increase stability of gadolinium-based magnetic resonance imaging contrast agents. Nat Commun [Internet]. 2019;10:1420. Available from: http://www.nature.com/articles/s41467-019-09342-3.
3. Le Fur M, Caravan P. The biological fate of gadolinium-based MRI contrast agents: a call to action for bioinorganic chemists. Metallomics. 2019;11:240–54. Available from: https://academic.oup.com/metallomics/article/11/2/240-254/5957487.
4. Marangoni VS, Germano LD, Silva CCC, de Souza EA, Maroneze CM. Engineering two-dimensional gold nanostructures using graphene oxide nanosheets as a template. Nanoscale. 2018;10:13315–9. Available from: http://xlink.rsc.org/?DOI=C8NR02855A.
5. Sinha S, Tong WY, Williamson NH, McInnes SJP, Puttick S, Cifuentes-Rius A, et al. Novel Gd-loaded silicon nanohybrid: a potential epidermal growth factor receptor expressing cancer cell targeting magnetic resonance imaging contrast agent. ACS Appl Mater Interfaces. 2017;9:42601–11. https://doi.org/10.1021/acsami.7b14538.
6. Wahsner J, Gale EM, Rodríguez-Rodríguez A, Caravan P. Chemistry of MRI contrast agents: current challenges and new frontiers. Chem Rev. 2019;119:957–1057. https://doi.org/10.1021/acs.chemrev.8b00363.
7. Silva F, Cabral Campello MP, Paulo A. radiolabeled gold nanoparticles for imaging and therapy of cancer. Materials (Basel) [Internet]. 2020;14:4. Available from: https://www.mdpi.com/1996-1944/14/1/4.
8. Coughlin AJ, West JL. Targeting gold nanoparticles for cancer diagnostics and therapeutics. ACS Symp Ser. 2012. https://doi.org/10.1021/bk-2012-1113.ch003.
9. Zhan C, Huang Y, Lin G, Huang S, Zeng F, Wu S. A gold nanocage/cluster hybrid structure for whole-body multispectral optoacoustic tomography imaging, EGFR inhibitor delivery, and photothermal therapy. Small. 2019;15:1900309. https://doi.org/10.1002/smll.201900309.
10. Castilho ML, Hewitt KC, Raniero L. FT-IR characterization of a theranostic nanoprobe for photodynamic therapy and epidermal growth factor receptor targets. Sensors Actuators B Chem. 2017;240:903–8.
11. Castilho ML, Jesus VPS, Vieira PFA, Hewitt KC, Raniero L. Chlorin e6-EGF conjugated gold nanoparticles as a nanomedicine

based therapeutic agent for triple negative breast cancer. Photodiagn Photodyn Ther. 2021;33:102186.
12. Lucas LJ, Hewitt KC. Nanobiophotonics for molecular imaging of cancer: Au- and Ag-based epidermal growth factor receptor (EGFR) specific nanoprobes. In: Vo-Dinh T, Lakowicz JR, editors. Proc Plasmon Biol Med IX [Internet]. SPIE; 2012. p. 82340C. https://doi.org/10.1117/12.906794.
13. Lucas LJ, Tellez C, Castilho ML, Lee CLD, Hupman MA, Vieira LS, et al. Development of a sensitive, stable and EGFR-specific molecular imaging agent for surface enhanced Raman spectroscopy. J Raman Spectrosc. 2015;46:434–46. https://doi.org/10.1002/jrs.4678.
14. Lee PC, Meisel D. Adsorption and surface-enhanced Raman of dyes on silver and gold sols. J Phys Chem. 1982;86:3391–5. https://doi.org/10.1021/j100214a025.
15. Vieira L, Castilho ML, Ferreira I, Ferreira-Strixino J, Hewitt KC, Raniero L. Synthesis and characterization of gold nanostructured Chorin e6 for photodynamic therapy. Photodiagnosis Photodyn Ther. 2017;18:6–11.
16. Rohrer M, Bauer H, Mintorovitch J, Requardt M, Weinmann H-J. Comparison of magnetic properties of MRI contrast media solutions at different magnetic field strengths. Invest Radiol. 2005;40:715–24.
17. Abidi N, Cabrales L, Hequet E. Fourier transform infrared spectroscopic approach to the study of the secondary cell wall development in cotton fiber. Cellulose. 2010;17:309–20. https://doi.org/10.1007/s10570-009-9366-1.
18. Rajkumar K, Muthukumar M, Mangalaraja RV. Electrochemical degradation of C.I. reactive orange 107 using gadolinium (Gd3+), neodymium (Nd3+) and samarium (Sm3+) doped cerium oxide nanoparticles. Int J Ind Chem. 2015;6:285–95. https://doi.org/10.1007/s40090-015-0051-y.
19. Zhang L, Liu T, Xiao Y, Yu D, Zhang N. Hyaluronic acid-chitosan nanoparticles to deliver Gd-DTPA for MR cancer imaging. Nanomaterials. 2015;5:1379–96. Available from: https://www.mdpi.com/journal/nanomaterials.
20. Bhattacharjee TT, Castilho ML, de Oliveira IR, Jesus VPS, Hewitt KC, Raniero L. FTIR study of secondary structure changes in epidermal growth factor by gold nanoparticle conjugation. Biochim Biophys Acta Gen Subj. 2018;1862:495–500.
21. Silverstein RM, Webster FX, Kiemle DJ. Spectrometric identification of organic compounds. 7th ed. Rio de Janeiro: LTC; 2007.
22. Coates J. Interpretation of infrared spectra, a practical approach. In: Meyer RA, editor. Encycl. of analytical chem. Wiley: New York; 2006. p. 10815–37.
23. Wan F, Wang L, Xu W, Li C, Li Y, Zhang C, et al. Binuclear gadolinium(III) complex based on DTPA and 1,3-bis(4-aminophenyl)adamantane as a high-relaxivity MRI contrast agent. Polyhedron. 2018;145:141–6. https://doi.org/10.1016/j.poly.2018.01.032.
24. Gao S, George SJ, Zhou Z-H. Interaction of Gd-DTPA with phosphate and phosphite: toward the reaction intermediate in nephrogenic systemic fibrosis. Dalton Trans [Internet]. 2016;45:5388–94. Available from: http://xlink.rsc.org/?DOI=C5DT04172D.
25. Tavakkoli Yaraki M, Tayebi M, Ahmadieh M, Tahriri M, Vashaee D, Tayebi L. Synthesis and optical properties of cysteamine-capped ZnS quantum dots for aflatoxin quantification. J Alloys Compd. 2017;690:749–58.
26. Rozenberg M, Lansky S, Shoham Y, Shoham G. Spectroscopic FTIR and NMR study of the interactions of sugars with proteins. Spectrochim Acta Part A Mol Biomol Spectrosc. 2019;222:116861.
27. Smith B. Infrared Spect Interpret [Internet]. 1998. Available from: https://www.taylorfrancis.com/books/9781351438384.
28. Sakellari GI, Hondow N, Gardiner PHE. Factors influencing the surface functionalization of citrate stabilized gold nanoparticles with cysteamine, 3-mercaptopropionic acid or l-selenocystine for sensor applications. Chemosensors [Internet]. 2020;8:80. Available from: https://www.mdpi.com/2227-9040/8/3/80.
29. Fagundes J, Castilho ML, Téllez Soto CA, Vieira LDS, Canevari RA, Fávero PP, et al. Ribosomal DNA nanoprobes studied by Fourier transform infrared spectroscopy. Spectrochim Acta Part A Mol Biomol Spectrosc. 2014;118:28–35.
30. Kumar S, Meena VK, Hazari PP, Sharma SK, Sharma RK. Rose Bengal attached and dextran coated gadolinium oxide nanoparticles for potential diagnostic imaging applications. Eur J Pharm Sci. 2018;117:362–70.
31. Fauzia RP, Mutalib A, Soedjanaatmadja RUMS, Bahti HH, Anggraeni A, Gunawan AH, et al. Synthesis and characterization of gadolinium diethylenetriamine pentaacetate-folate. Procedia Chem. 2015;17:139–46.
32. Zhou W, Shen J, Lin J, An M, An L, Tian Q, et al. Zeolitic imidazolate framework nanoparticles loaded with gadolinium chelate as efficient T1 MRI contrast agent. J Mater Sci. 2021;56:7386–96. https://doi.org/10.1007/s10853-020-05647-7.
33. Lu R, Zhang Y, Tao H, Zhou L, Li H, Chen T, et al. Gadolinium-hyaluronic acid nanoparticles as an efficient and safe magnetic resonance imaging contrast agent for articular cartilage injury detection. Bioact Mater. 2020;5:758–67.
34. Li K, Wen, Larson AC, Zhang Z, Shen, Chen, et al. Multifunctional dendrimer-based nanoparticles for in vivo MR/CT dual-modal molecular imaging of breast cancer. Int J Nanomedicine [Internet]. 2013;8:2589. Available from: http://www.dovepress.com/multifunctional-dendrimer-based-nanoparticles-for-in-vivo-mrct-dual-mo-peer-reviewed-article-IJN.
35. Dutra BG, Bauab T Jr. MEIOS DE CONTRASTE Conceitos e diretrizes. In: Garbugio Dutra B, Bauab T Jr, editors. MEIOS CONTRASTE Conceitos e diretrizes. São Caetano do Sul. São Paulo: Farol Editora; 2022. https://doi.org/10.46664/meios-de-contraste.
36. Mazzola AA, Stieven KI, Neto GH, Cardoso GDM. Segurança em Imagem por Ressonância Magnética. Rev Bras Física Médica [Internet]. 2019;13:76. Available from: http://www.rbfm.org.br/rbfm/article/view/519.
37. Sherry AD, Wu Y. The importance of water exchange rates in the design of responsive agents for MRI. Curr Opin Chem Biol. 2013;17:167–74.
38. Ferreira MF, Mousavi B, Ferreira PM, Martins CIO, Helm L, Martins JA, et al. Gold nanoparticles functionalised with stable, fast water exchanging Gd3+ chelates as high relaxivity contrast agents for MRI. Dalt Trans. 2012;41:5472–5.
39. Costelloe CM, Amini B, Madewell JE. Risks and benefits of gadolinium-based contrast-enhanced MRI. Semin Ultrasound CT MRI. 2020;41:170–82.
40. Heydarnezhadi S, Riahi Alam N, Haghgoo S, Ghanaati H, Khoobi M, Gorji E, et al. Glycosylated gadolinium as potential metabolic contrast agent vs Gd-DTPA for metabolism of tumor tissue in magnetic resonance imaging. Appl Magn Reson. 2016;47:375–85.
41. da Silva YLP, Costa RZV, Pinho KEP, Ferreira RR, Schuindt SM. Effects of iodinated contrast agent, xylocaine and gadolinium concentration on the signal emitted in magnetic resonance arthrography: a samples study. Radiol Bras [Internet]. 2015;48:69–73. Available from: http://www.scielo.br/scielo.php?script=sci_arttext&pid=S0100-39842015000200005&lng=en&tlng=en.
42. Wei Z, Ma Y-J, Jang H, Yang W, Du J. To measure T1 of short T2 species using an inversion recovery prepared three-dimensional ultrashort echo time (3D IR-UTE) method: a phantom study. J Magn Reson. 2020;314:106725.
43. Mundim JS, Lorena SDC, Abensur H, Elias RM, Moysés RMA, de Castro MCM, et al. Fibrose sistêmica nefrogênica: Uma complicação grave do uso do gadolínio em pacientes com insuficiência renal. Rev Assoc Med Bras. 2009;55:220–5.

44. Runge VM. Safety of the gadolinium-based contrast agents for magnetic resonance imaging, focusing in part on their accumulation in the brain and especially the dentate nucleus. Invest Radiol. 2016;51:273–9.
45. Acharya S, Dilnawaz F, Sahoo SK. Targeted epidermal growth factor receptor nanoparticle bioconjugates for breast cancer therapy. Biomaterials. 2009;30:5737–50.
46. Creixell M, Bohórquez AC, Torres-Lugo M, Rinaldi C. EGFR-targeted magnetic nanoparticle heaters kill cancer cells without a perceptible temperature rise. ACS Nano. 2011;5:7124–9. https://doi.org/10.1021/nn201822b.